

LETTER TO THE EDITOR

Detection of the magnetar XTE J1810–197 at 150 and 260 GHz with the NIKA2 Kinetic Inductance Detector camera

P. Torne^{1,2*}, J. Macías-Pérez³, B. Ladjelate¹, A. Ritacco^{1,4,5}, M. Sánchez-Portal¹, S. Berta⁶, G. Paubert¹, M. Calvo⁷, G. Desvignes^{8,9}, R. Karuppusamy⁹, S. Navarro¹, D. John¹, S. Sánchez¹, J. Peñalver¹, M. Kramer^{9,10}, and K. Schuster⁶

¹ Instituto de Radioastronomía Milimétrica (IRAM), Avda. Divina Pastora 7, Local 20, 18012 Granada, Spain

² East Asian Observatory, 660 N. A'ohoku Place, University Park, Hilo, Hawaii 96720, USA

³ Laboratoire de Physique Subatomique et de Cosmologie, Université Grenoble-Alpes, CNRS, 53 av. des Martyrs, 38026 Grenoble, France

⁴ Institut d'Astrophysique Spatiale (IAS), CNRS and Université Paris-Sud, Bâtiment 121, Orsay, France

⁵ Laboratoire de Physique de l'École Normale Supérieure, ENS, 24 rue Lhomond, 75005 Paris, France

⁶ Institut de Radioastronomie Millimétrique (IRAM), 300 rue de la Piscine, 38406 St. Martin d'Hères, France

⁷ Institut Néel, CNRS and Université Grenoble-Alpes, 25 rue des Martyrs BP 166, 38042 Grenoble, France

⁸ LESIA, Observatoire de Paris, Université PSL, CNRS, Sorbonne Université, Université de Paris, 5 place Jules Janssen, 92195 Meudon, France

⁹ Max-Planck-Institut für Radioastronomie, Auf dem Hügel 69, D-53121, Bonn, Germany

¹⁰ Jodrell Bank Centre for Astrophysics, School of Physics and Astronomy, University of Manchester, Manchester M13 9PL, UK

Received May 27, 2020; accepted July 3, 2020

ABSTRACT

Context. The investigation of pulsars between millimetre and optical wavelengths is challenging due to the faintness of the pulsar signals and the relative low sensitivity of the available facilities compared to 100-m class telescopes operating in the centimetre band. The Kinetic Inductance Detector (KID) technology offers large instantaneous bandwidths and a high sensitivity that can help to substantially increase the ability of existing observatories at short wavelengths to detect pulsars and transient emission.

Aims. To investigate the feasibility of detecting pulsars with KIDs, we observed the anomalous X-ray pulsar XTE J1810–197 with the New IRAM KIDs Array-2 (NIKA2) camera installed at the IRAM 30-m Telescope in Spain.

Methods. Several short observations of XTE J1810–197 were made on 2019 March 25 under good weather conditions to verify the stability of the KIDs and to try to detect the expected broadband pulsations from the neutron star.

Results. We detected the pulsations from the pulsar with NIKA2 at its two operating frequency bands, 150 and 260 GHz ($\lambda=2.0$ and 1.15 mm, respectively). This is the first time that a pulsar is detected with a receiver based on KID technology in the millimetre band. In addition, this is the first report of short millimetre emission from XTE J1810–197 after its reactivation in December 2018, and it is the first time that the source is detected at 260 GHz, which gives us new insights into the radio emission process of the star.

Conclusions. We demonstrate that KIDs can fulfil the technical requirements to detect pulsed emission from neutron stars in the millimetre band and show that the magnetar XTE J1810–197 is again emitting strong pulsations in the short millimetre band.

Key words. Stars: magnetars – (Stars:) pulsars: individual XTE J1810–197 – Instrumentation: detectors – Astronomical instrumentation, methods and techniques – Radiation mechanisms: non-thermal

1. Introduction

Pulsars are rotating neutron stars that emit broadband beamed emission, detectable as pulses from Earth as their beams cross our line-of-sight. They act like cosmic clocks and their study enable high-precision astronomy (e.g., Kramer et al. 2006; Eatough et al. 2013; Cromartie et al. 2020). Nevertheless, their coherent radio emission mechanism is still unknown (for a review, see e.g., Melrose 2017).

One way to help better understanding the coherent and incoherent components of pulsar emission and aid constraining theoretical models is to measure their spectrum in the poorly explored window between the radio and optical regimes (e.g., Michel 1978). However, pulsars are in general steep spectral sources in the radio band, making their emission extremely weak above a few GHz (Maron et al. 2000). Additionally, as frequency

increases, the collecting areas and efficiency of the available telescopes tend to decrease, and instrumentation with enough time resolution to resolve the pulsations is rarely available. As a result, pulsar studies in the millimetre, infrared, and optical regimes are sparse and highly challenging.

To improve our ability to detect and study pulsars at short wavelengths, we need higher sensitivity. One solution is to use large-bandwidth and low-noise receivers. In recent years, a new technology based on Kinetic Inductance Detectors (KIDs) has been used to fabricate sensitive large-array detectors (for a review, see Mauskopf 2018). Indeed, KID arrays of thousands of pixels can be built and operated with state-of-art sensitivity (Monfardini et al. 2011; Mazin et al. 2013; Catalano et al. 2014; Calvo et al. 2016; Perotto et al. 2020).

Furthermore, KIDs are fast detectors, with typical time constants of the order 100 μ s (Catalano et al. 2016; Monfardini et al. 2016), and can be used at very high sampling rates up to few

* Main contact author, e-mail: torne@iram.es

MHz (Swenson et al. 2010; Bourrion et al. 2016; Fasano et al. 2020). Hence, KIDs are a promising tool to investigate pulsars in unexplored sections of their spectrum and test models of pulsar magnetospheres.

The KID-based NIKA2 camera installed at the IRAM 30-m Telescope (Adam et al. 2018) is a dual wide band camera operating simultaneously at 150 and 260 GHz ($\lambda=2.0$ and 1.15 mm) with 45 GHz of bandwidth and a total of 2896 KIDs cooled down at about 150 mK (Calvo et al. 2016). NIKA2 offers an excellent performance with typical sensitivities per detector of 9 and 30 mJy s^{1/2} at 150 and 260 GHz, respectively (Perotto et al. 2020). In the future, NIKA2 will also offer polarisation measurements in the 260-GHz band (Ritacco et al. 2020). Currently, NIKA2 maximum theoretical sampling frequency is 500 Hz¹.

The observations presented here focus on the anomalous X-ray pulsar XTE J1810–197. This pulsar was identified as a magnetar in 2003 after a sudden increase in its X-ray luminosity (Ibrahim et al. 2004). Magnetars are a small family of pulsars whose high-energy luminosity cannot be accounted for solely by the spindown energy, and thought to be powered in addition by magnetic field decay (for a review on magnetar properties see e.g., Kaspi & Beloborodov 2017). XTE J1810–197 was furthermore the first magnetar found to exhibit radio emission (Halpern et al. 2005; Camilo et al. 2006), an uncommon property that only five of the known 23 known magnetars have shown to date. Interestingly, and in contrast to the majority of the pulsar population, radio magnetars share a tendency to maintain a flat or even inverted spectrum in the radio band (Levin et al. 2010; Camilo et al. 2007, 2008; Torne et al. 2015). Therefore, radio magnetars can be very bright in the millimetre band (Torne et al. 2017).

XTE J1810–197 is highly variable and ceased its radio emission about three years after the discovery of the radio pulsations (Camilo et al. 2016). However, radio emission from the neutron star was re-detected in December 2018 (Levin et al. 2019), and follow-up campaigns at several wavelengths including X-ray (Gotthelf et al. 2019) confirmed that the source entered a new period of intense radiative activity. Observations were also carried out with the Superconductor-Insulator-Superconductor (SIS) Eight Mixer Receiver (EMIR, Carter et al. 2012) at the IRAM 30-m Telescope, confirming that the source was also bright in the millimetre band. Those observations will be presented elsewhere, but confirmed that XTE J1810–197 was a good candidate to try its observation with NIKA2 and test the ability of the KIDs to detect broadband pulsations in the millimetre band.

2. Dataset and Methods

2.1. Observations

The observations of XTE J1810–197 were done on 2019 March 25 with the NIKA2 camera at the IRAM 30-m Telescope under good weather conditions ($\tau_z^{225\text{ GHz}} = 0.29$). The KID arrays were configured to sample at a standard frequency $F_s = 23.84$ Hz, enough to obtain 132 data points across one rotational period of the pulsar ($P \approx 5.54$ s). The observing mode was set to “stare mode”, in which the telescope tracked continuously the source at a fixed position on the three arrays of the camera.

In NIKA2, the resonance frequency of each detector is proportional to the input signal, and signal variations translate into resonance shifts. During the observations we measure the signal via the amplitude and phase shift (transfer function) of a specific

microwave test tone for each detector (Calvo et al. 2016). Prior to an observation, the detectors and readout are tuned to adapt the response to the input background signal from the sky. To ensure a coherent time series the data were acquired continuously during each full scan and recorded into a single data file.

In total, we recorded four scans on XTE J1810–197, the first two with 10 min of duration each and the last two with 15 min duration each. The maximum integration time per scan was set to ensure efficient and manageable data processing.

2.2. Data processing

The exact position of the magnetar on the KID arrays was a priori only known to a certain precision. To search for the exact pixels on which the source was centred, we wrote as 32-bit-float time series the values of reconstructed signal (in resonance frequency units) from a number of pixels around the estimated position, corresponding to an area on sky of about 1 arcmin². Because the pixel size and separation are different for the 2 and 1.15 mm arrays, time series from 45 pixels (slightly larger area) were extracted for the 2 mm array (named A2), and 77 and 84 pixels for the two arrays at 1.15 mm (named A1 and A3, respectively). The difference in the number of pixels for the two 1.15 mm arrays is due to a slightly larger number of non-valid pixels in array A3 (Perotto et al. 2020).

Next, we filtered the time series to subtract the atmospheric variations. We applied a “running-fit” filter consisting of a moving window of 4.5 s. As the window moves, a first-order polynomial is fit and subtracted to the data. Each filtered time series (i.e., from each extracted KID pixel) was then directly folded by the routine `prepfold` from the pulsar analysis suite `PRESTO`². An ephemeris from Camilo et al. (2016), obtained from the pulsar database `PSRCAT`³ (Manchester et al. 2005), was used to predict the spin period at the epoch of the observations. The resulting pulsar candidate plots were manually inspected to identify the time series, and so the KID pixel of each array, that contained the best signal in terms of signal-to-noise at the spin period of XTE J1810–197. The KID pixels containing the highest-significance pulsations were KH097, KC016, and KP018, for the A1, A2, and A3 array, respectively.

A running-fit (or running-median or mean) filtering tends to subtract part of the pulsar signal, affecting the intensity measurements. For this reason, once the pixels containing the magnetar signal were identified, we re-processed the data using a so-called “multi-pixel filter”. This method exploits the advantage of having multiple beams on the sky to remove the atmospheric variations while preserving the pulsation unaffected. For 150 GHz, we selected pixels pointed on the sky between 2 and 3 Half-Power Beam Widths (HPBW, $\theta_{150} \approx 17.7$ arcsec) around the magnetar. At 260 GHz, since the detectors are less sensitive and the atmospheric fluctuations larger, we selected pixels pointing somewhat closer, between 1.25 and 2.5 HPBWs ($\theta_{260} \approx 11.2$ arcsec). From this subset, the pixels showing residual pulsations at any signal-to-noise (as found with the running-fit filter) are flagged and excluded from the analysis. For the remaining (17 pixels for A2, 14 pixels for A1 and A3), a running median with a window of 1.5 s is applied, and the resulting running median vectors are averaged and subtracted from the time series centred on the magnetar. This is done separately for arrays A1, A2, and A3. The time series at 260 GHz still show some residual slow fluctuations after this procedure. In these cases, a final smoothing by a running median

² <https://www.cv.nrao.edu/~sransom/presto/>

³ <https://www.atnf.csiro.au/research/pulsar/psrcat/>

¹ This fast-sampling mode is pending commissioning.

Table 1. XTE J1810–197 measured properties at the epoch of observation (2019 March 25): MJD epoch, barycentered spin period, continuum-equivalent flux density at 150 and 260 GHz, and spectral index. Uncertainties in parenthesis indicate the 1- σ error on the last significant quoted digit.

Epoch (MJD)	P (s)	S_{150} (mJy)	S_{260} (mJy)	α
58567.23714	5.541396(3)	11.7(7)	6.4(10)	-1.1(3)

of window 5 s was applied. This filtering method resulted in a clean average profile with a flat off-pulse region, and without the typical dips resulting from direct running median or running fit subtractions.

Finally, the time series cleaned by the multi-pixel filter were reformatted as SIGPROC⁴ filterbank-type files by adding a header containing the metadata of the observation. The binary formatting of the header was done with tools from SIGPYPROC⁵. Then, to increase the total signal-to-noise, the four individual scans were concatenated letting `prepfold` to pad the gaps in between scans. For the 260 GHz frequency, arrays A1 and A3 receive half of the total power each. Thus, prior to the concatenation and folding, the time series from the orthogonal linearly polarised pixels KH097 and KP018 were combined to produce the total intensity output.

2.3. Calibration

To convert to flux density units, and prior to the analysis presented in Sec. 2.2, we scaled the time series by calibration factors obtained from observations of planet Uranus taken in September 2018 and March 2019 (see Perotto et al. 2020, for details in NIKA2 calibration). These observations were also used to compute the relative sky position between detectors. A correction was applied to the intensity at 260 GHz to account for a slight misalignment of the beams from pixels KH097 and KP018 with respect to the position on sky of pixel KC016. The distance between the beams at 150 and 260 GHz for the utilised pixels was 4.5 arcsec. The correction includes a pointing offset of 2 arcsec from the magnetar position. The beam misalignment plus pointing offset result in an increase of a factor of two for the 260-GHz intensity. The uncertainties are derived from the noise statistics, combined with a 6 and 10 percent 1- σ error for the 150 and 260-GHz bands, respectively, originating from the scaling-to-Jansky factors (Perotto et al. 2020), combined with a 10 percent 1- σ error for the correction due to the misalignment of the beams.

3. Results and Discussion

The magnetar XTEJ1810–197 was clearly detected in both bands of the NIKA2 camera at central frequencies 150 and 260 GHz ($\lambda=2.0$ and 1.15 mm), with peak significance of 124σ and 13σ , respectively. Figure 1 shows the average profiles and signal intensities as a function of integration time. At 150 GHz we detect individual pulsations in almost every rotation of the magnetar (see Fig. 2).

Table 1 presents the continuum-equivalent (or averaged) flux density (i.e., the area under the pulse divided by the rotational period) and derived spectral index. The spectrum and fit is shown in Figure 3. With $S_{150} = 11.7 \pm 0.7$ mJy and $S_{260} = 6.4 \pm 1.0$ mJy, the average spectral index is $\alpha = -1.1 \pm 0.3$ (for $S_\nu \propto \nu^\alpha$). Due to the low number of data points and to better estimate the uncertainties, the spectral index was fit via a Markov Chain Monte Carlo (MCMC) analysis using the Python package `emcee`⁶ (Foreman-Mackey et al. 2013).

The resulting spectrum is relatively flat, although much steeper than the inverted spectrum measured between 0.7–4.0 GHz ($\alpha \approx +0.3$, Dai et al. 2019). The millimetre flux density is about ~ 9 times higher compared to what can be estimated from the light curve reported by Maan et al. (2019) (≈ 1.0 mJy at 650 MHz). If we include this low-frequency value, the spectral fit would result in $\alpha \approx +0.39 \pm 0.02$, consistent with the derived value at lower frequency. The difference in spectral index resulting from using only the millimetre data could be related to a poor constraint of the fit with only two data points. However, interstellar scintillation (see discussion in Lazaridis et al. 2008) and/or a frequency-dependent intrinsic variability of the magnetar emission may also play a role. In fact, we measure variations of the flux density of up to 50% peak-to-peak during our observations (in scales of tens of minutes). Jointly, we should consider that the spectrum of XTEJ1810–197 may not always be well described over large frequency ranges by a single power law, something consistent with the spectral turnover reported by Dai et al. (2019), and observed for other radio magnetars (Camilo et al. 2008; Torne et al. 2017). A conclusive answer on the spectral shape between centimetre and millimetre wavelengths, which would enable tests of the radio emission mechanism (for instance revealing spectral turn-ups, Michel 1978), requires simultaneous multi-frequency observations.

The single pulsations at 150 GHz allow for an estimation of the brightness temperature of the emission region, enabling to test if the millimetre emission is still coherent. For a distance to XTEJ1810–197 of 3.5 ± 0.5 kpc (Minter et al. 2008) and a typical detected 0.75 Jy pulse, the brightness temperature at 150 GHz is $T_B > 10^{17}$ K (see e.g., Lorimer & Kramer 2005). We set the value as a lower limit because the pulses are not resolved, and narrower pulses correspond (following a light-travel-time argument) to smaller emitting regions and higher brightness temperatures. Even at the lower limit, such high brightness temperature rule out incoherent mechanisms for the production of the pulses (e.g., Singal 2009). We conclude therefore that the underlying mechanism responsible for the emission at 150 GHz must still keep a level of coherency. At 260 GHz, with no detected single pulses, we cannot constrain the emission mechanism. We hypothesise, however, that being the continuum-equivalent flux density and pulse profile so similar between the two frequency bands, the 260-GHz emission probably arises from the same emission process. Additional higher-time-resolution observations are encouraged, which could help to further constrain the coherency of the emission mechanism by detecting narrower pulses⁷, perhaps also at 1.15 mm or even shorter wavelengths.

While in the 2 mm band XTEJ1810–197 was already detected during its previous epoch of activity in 2006 (at 144 GHz, $\lambda=2.08$ mm, Camilo et al. 2007), this is the first detection of the source at 260 GHz ($\lambda=1.15$ mm). The fact that we see again strong emission from XTEJ1810–197 in the millimetre band as

⁴ <http://sigproc.sourceforge.net>

⁵ <https://github.com/ewanbarr/sigpyproc>

⁶ <https://emcee.readthedocs.io/>

⁷ Time scales for individual pulses at lower frequencies are $\lesssim 1$ ms (Maan et al. 2019).

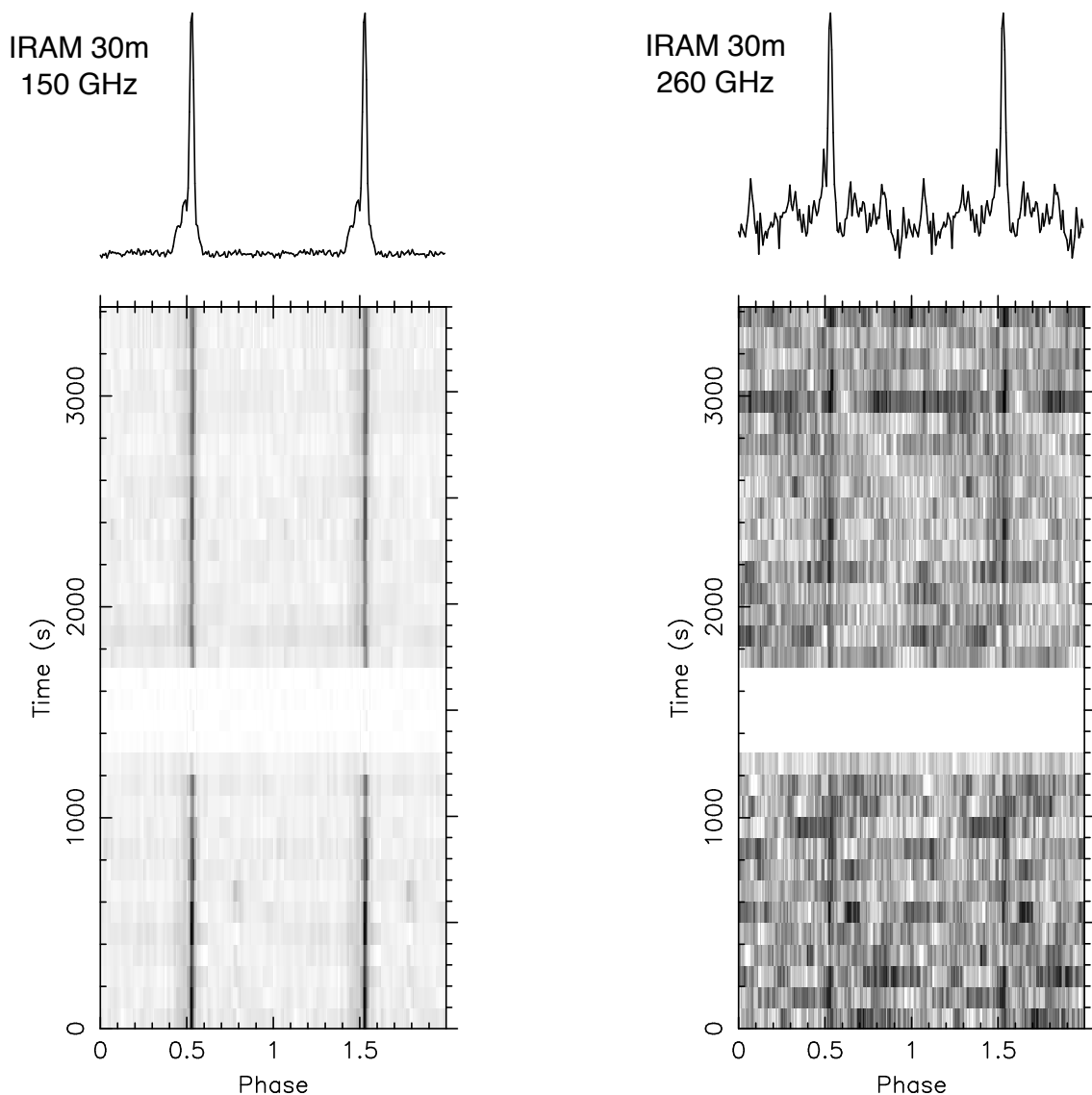


Fig. 1. Average profiles (shown twice for clarity) of the detection of XTE J1810-197 with NIKA2 at 150 GHz (left) and 260 GHz (right). Profiles have 128 bins, corresponding to a time resolution of ≈ 43 ms on the horizontal axis. The bottom panels show the signal intensity over time with 1.7-min resolution on the vertical axis. The white gap corresponds to time when the telescope was not observing the source.

in 2006, suggests that the radio emission process reactivated now is the same as in the previous period of activity. In the 2 mm band, however, the emission is ~ 10 times stronger than what was reported by Camilo et al. (2007).

The results presented here demonstrate that XTE J1810-197 is producing strong pulsed emission in the millimetre band after its reactivation in December 2018. Given the intrinsic variability of the source, XTE J1810-197 is opening a new opportunity to investigate the properties of pulsar emission at short millimetre wavelengths, where only another radio magnetar and two canonical pulsars have been detected above 50 GHz (Torne et al. 2015, 2017; Morris et al. 1997; Torne 2017; Liu et al. 2019). Given the current intensity and activity of this magnetar, even shorter-wavelength observations covering submillimetre to optical bands are encouraged.

Finally, we remark that this is the first time that KID technology as used in NIKA2 is successfully applied to detect broadband pulsations from neutron stars in the millimetre wavelength regime. In the future, the sampling frequency of NIKA2 may be

increased, allowing for observations of faster-spinning pulsars or even burst emission of the kind of Fast Radio Bursts (FRB, see e.g., Cordes & Chatterjee 2019).

4. Conclusions

1. Kinetic Inductance Detector (KID) technology has the capability to detect pulsations from neutron stars in the millimetre band, as demonstrated by these results on the magnetar XTE J1810-197 with the NIKA2 camera installed at the IRAM 30-m Telescope. Similarly, KIDs may be applicable at even shorter wavelengths for observing pulsars and transient emission.
2. The detection of XTE J1810-197 at 150 and 260 GHz ($\lambda=2.0$ and 1.15 mm, respectively) are the first detection of the magnetar above 144 GHz, showing that the star is again emitting intense millimetre radiation after its reactivation in December 2018. The spectrum in the millimetre band is relatively flat, although steeper than what was seen at centimetre

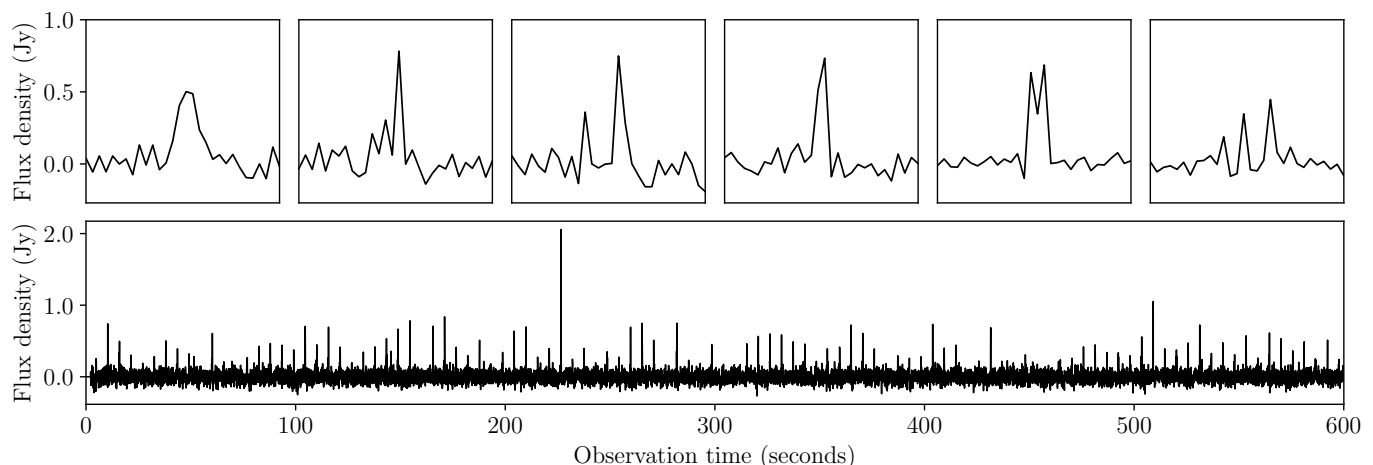


Fig. 2. Single pulse activity from XTE J1810–197 during our observations with NIKA2 on 2019 March 25. Only the last 10 min of the observation at 150 GHz are shown for clarity, but the activity is similar for the total 50 min on-source. No single pulses are detected at 260 GHz, which may be an effect of both spectral index and instrumental sensitivity. Upper panels show a zoom (1.25 s around the peak) into a selection of six pulses, and share the y-axis scale in Jansky units. Bottom panel show the 10-min time series. The time resolution in all panels is ≈ 42 ms, limited by the sampling frequency set for the KID arrays. Structure can be seen in many pulses, with most of them unresolved.

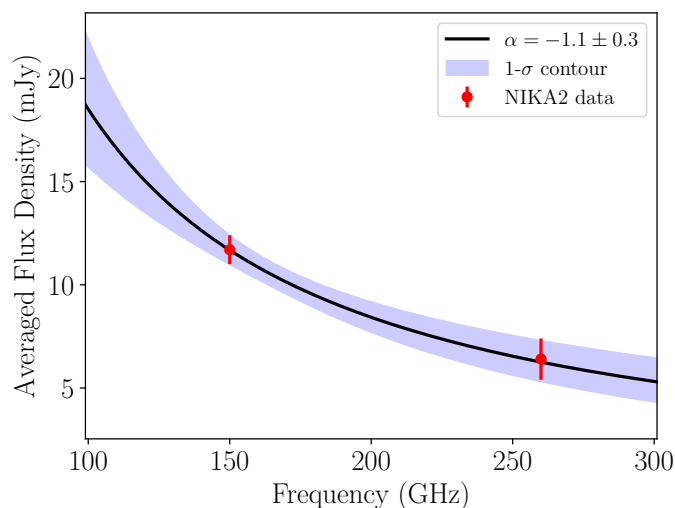


Fig. 3. Spectrum of emission in the millimetre band of the radio magnetar XTE J1810–197 during the observations with NIKA2 on 2019 March 25. The black solid line indicates the mean value, and the blue shaded region encompasses the 68% confidence interval. The spectral index is $\alpha = -1.1 \pm 0.3$ (for $S_\nu \propto \nu^\alpha$).

wavelengths. The brightness temperature of the individual pulsations support a coherent mechanism as the source of the millimetre emission.

Acknowledgements. We thank the anonymous referee, Clemens Thum and Carsten Kramer for their constructive comments on the manuscript, and the NIKA2 team for supporting the observations. This work is based on observations carried out with the IRAM 30-m telescope. IRAM is supported by INSU/CNRS (France), MPG (Germany) and IGN (Spain). Financial support by the European Research Council for the ERC Synergy Grant BlackHoleCam (ERC-2013-SyG, Grant Agreement no. 610058) is gratefully acknowledged.

References

- Adam, R., Adane, A., Ade, P. A. R., et al. 2018, *A&A*, 609, A115
 Bourrion, O., Benoit, A., Bouly, J. L., et al. 2016, *Journal of Instrumentation*, 11, P11001

- Calvo, M., Benoit, A., Catalano, A., et al. 2016, *Journal of Low Temperature Physics*, 184, 816
 Camilo, F., Ransom, S. M., Halpern, J. P., et al. 2016, *ApJ*, 820, 110
 Camilo, F., Ransom, S. M., Halpern, J. P., et al. 2006, *Nature*, 442, 892
 Camilo, F., Ransom, S. M., Peñalver, J., et al. 2007, *ApJ*, 669, 561
 Camilo, F., Reynolds, J., Johnston, S., Halpern, J. P., & Ransom, S. M. 2008, *ApJ*, 679, 681
 Carter, M., Lazareff, B., Maier, D., et al. 2012, *A&A*, 538, A89
 Catalano, A., Benoit, A., Bourrion, O., et al. 2016, *A&A*, 592, A26
 Catalano, A., Calvo, M., Ponthieu, N., et al. 2014, *A&A*, 569, A9
 Cordes, J. M. & Chatterjee, S. 2019, *ARA&A*, 57, 417
 Cromartie, H. T., Fonseca, E., Ransom, S. M., et al. 2020, *Nature Astronomy*, 4, 72
 Dai, S., Lower, M. E., Bailes, M., et al. 2019, *ApJ*, 874, L14
 Eatough, R. P., Falcke, H., Karuppusamy, R., et al. 2013, *Nature*, 501, 391
 Fasano, A., Aguiar, M., Benoit, A., et al. 2020, *Journal of Low Temperature Physics*, 199, 529
 Foreman-Mackey, D., Conley, A., Meierjürgen Farr, W., et al. 2013, *emcee: The MCMC Hammer*, *Astrophysics Source Code Library*
 Gotthelf, E. V., Halpern, J. P., Alford, J. A. J., et al. 2019, *ApJ*, 874, L25
 Halpern, J. P., Gotthelf, E. V., Becker, R. H., Helfand, D. J., & White, R. L. 2005, *ApJ*, 632, L29
 Ibrahim, A. I., Markwardt, C. B., Swank, J. H., et al. 2004, *ApJ*, 609, L21
 Kaspi, V. M. & Beloborodov, A. M. 2017, *ARA&A*, 55, 261
 Kramer, M., Stairs, I. H., Manchester, R. N., et al. 2006, *Science*, 314, 97
 Lazaridis, K., Jessner, A., Kramer, M., et al. 2008, *MNRAS*, 390, 839
 Levin, L., Bailes, M., Bates, S., et al. 2010, *ApJ*, 721, L33
 Levin, L., Lyne, A. G., Desvignes, G., et al. 2019, *MNRAS*, 488, 5251
 Liu, K., Young, A., Wharton, R., et al. 2019, *ApJ*, 885, L10
 Lorimer, D. R. & Kramer, M. 2005, *Handbook of Pulsar Astronomy*
 Maan, Y., Joshi, B. C., Surmis, M. P., Bagchi, M., & Manoharan, P. K. 2019, *ApJ*, 882, L9
 Manchester, R. N., Hobbs, G. B., Teoh, A., & Hobbs, M. 2005, *AJ*, 129, 1993
 Maron, O., Kijak, J., Kramer, M., & Wielebinski, R. 2000, *A&AS*, 147, 195
 Maukopf, P. D. 2018, *PASP*, 130, 082001
 Mazin, B. A., Meeker, S. R., Strader, M. J., et al. 2013, *PASP*, 125, 1348
 Melrose, D. B. 2017, *Reviews of Modern Plasma Physics*, 1, 5
 Michel, F. C. 1978, *ApJ*, 220, 1101
 Minter, A. H., Camilo, F., Ransom, S. M., Halpern, J. P., & Zimmerman, N. 2008, *ApJ*, 676, 1189
 Monfardini, A., Baselmans, J., Benoit, A., et al. 2016, *Society of Photo-Optical Instrumentation Engineers (SPIE) Conference Series*, Vol. 9914, Lumped element kinetic inductance detectors for space applications, 99140N
 Monfardini, A., Benoit, A., Bidaud, A., et al. 2011, *ApJS*, 194, 24
 Morris, D., Kramer, M., Thum, C., et al. 1997, *A&A*, 322, L17
 Perotto, L., Ponthieu, N., Macías-Pérez, J. F., et al. 2020, *A&A*, 637, A71
 Ritacco, A., Adam, R., Ade, P., et al. 2020, in *European Physical Journal Web of Conferences*, Vol. 228, mm Universe @ NIKA2 - Observing the mm Universe with the NIKA2 Camera, 00022
 Singal, A. K. 2009, *ApJ*, 703, L109
 Swenson, L. J., Cruciani, A., Benoit, A., et al. 2010, *Applied Physics Letters*, 96, 263511
 Torne, P. 2017, PhD thesis, University of Bonn
 Torne, P., Desvignes, G., Eatough, R. P., et al. 2017, *MNRAS*, 465, 242
 Torne, P., Eatough, R. P., Karuppusamy, R., et al. 2015, *MNRAS*, 451, L50